Article

JOURNAL OF COMPOSITE MATERIALS

Journal of Composite Materials
2014, Vol. 48(5) 571–592

DOI: 10.1177/0021998313476324
jcm.sagepub.com

SAGE

A failure-mode based anisomorphic constant life diagram for a unidirectional carbon/epoxy laminate under off-axis fatigue loading at room temperature

M Kawai and N Itoh

Abstract

The off-axis constant fatigue life diagrams for a unidirectional carbon/epoxy laminate in different fiber orientations are identified over the whole range of stress ratio. The experimental results show that the off-axis constant fatigue life diagram plotted in the plane of alternating and mean stresses tends to shrink and incline to the left of the alternating stress axis more significantly as the off-axis angle of a specimen increases. The overall shapes of the off-axis constant fatigue life envelopes for different constant values of life are highly non-linear and asymmetric about the alternating stress axis, regardless of fiber orientation. These observations suggest that the sensitivity to mean stress in off-axis fatigue differs depending on the mode of fatigue loading, i.e. tension–tension, tension–compression, and compression–compression loading, and the difference is associated with the different modes of failure under different modes of fatigue loading. To deal with the off-axis fatigue strength of a unidirectional composite for any fiber orientation over the whole range of stress ratio, a most general form of the anisomorphic constant fatigue life diagram is developed that can take into account different sensitivities to mean stress in fatigue and distinguish between the tensile- and compressive-dominated failure modes. It is demonstrated that the generalized anisomorphic constant fatigue life diagram allows accommodating itself to a significant change in shape of a constant fatigue life envelope that depends on the range of stress ratio, and thus it can successfully be applied to accurate description of the off-axis constant fatigue life diagram for the unidirectional carbon fiber reinforced plastic laminate, regardless of fiber orientation.

Keywords

Carbon fiber reinforced plastic, unidirectional laminate, off-axis fatigue, stress ratio, constant fatigue life diagram

Introduction

Engineering fatigue analysis of structural components made of carbon fiber reinforced plastic (CFRP) laminates is required to evaluate an allowable range of fatigue stress within which they do not fail. If an endurance limit is available below which no fatigue failure occurs in a CFRP laminate, it may be straightforward to define an allowable range of fatigue loading. For most CFRP laminates, however, their endurance limits in fatigue cannot clearly be identified. In the practice of engineering fatigue analysis of CFRP structures, therefore, an allowable range of fatigue stress should be defined as that within which they do not fail until a specified constant value of life. To implement it, we need the S–N relationships for the CFRP laminates employed in those structures, and thus, we need to identify them over a range of fatigue life. What should be reminded of is that the S–N relationship for a given CFRP laminate cannot uniquely be determined, but it depends on various factors that characterize fatigue loading, typically on the stress ratio of fatigue loading.[1–10] For fatigue analysis of CFRP structures, therefore, we have to determine the S–N relationships for the CFRP laminates employed in them at least under fatigue loading at different stress ratios.

Department of Engineering Mechanics and Energy, University of Tsukuba, Japan

Corresponding author:
M Kawai, Department of Engineering Mechanics and Energy, University of Tsukuba, Tsukuba 305-8573, Japan.
Email: mkawai@kz.tsukuba.ac.jp

A great number of fatigue tests are required in general to establish the *S–N* relationships for given CFRP laminates over the whole range of stress ratio and to identify their stress ratio dependence. Engineering fatigue analysis of composite structures necessitates relaxation of the requirement. Thus, we need to develop an efficient method for accurately evaluating the *S–N* relationships for composites for any stress ratios on the basis of a limited number of fatigue tests at carefully selected stress ratios. One of the most practical methods is to use a constant fatigue life (CFL) diagram that consists of the CFL envelopes for different constant values of life which are typically drawn in the plane of alternating stress and mean stress.[11,12] Once the CFL diagram for a given composite laminate is constructed, it allows graphically evaluating its fatigue life under constant amplitude fatigue loading at any stress ratio. Because of its practical importance, attention is increasingly focused on identification of the CFL diagrams for CFRP laminates over the whole range of mean stress. Recent experimental studies have shown that the CFL diagrams for CFRP laminates often exhibit significant non-linearity.[13–18] In their CFL diagrams, moreover, the maximum values of alternating stress often appear at non-zero mean stresses,[1,2,13–19] because of their different strengths in tension and compression. Accordingly, it is not always the case for CFRP laminates that a symmetric and linear CFL diagram of the Goodman[20] type can accurately describe the effect of mean stress on the fatigue life of a material over the whole range of mean stress.

These facts have encouraged developing an engineering method suitable for composites that allows describing the CFL diagrams for composites efficiently as well as accurately, which are asymmetric and non-linear in general, over the whole range of mean stress. Mandell et al.[21] and Sutherland and Mandell[22] presented modified Goodman diagrams that were built assuming linear interpolation of fatigue data at different stress ratios. Adam et al.[23] proposed an asymmetric parabolic representation of CFL envelopes for different constant values of life. Harris and other researchers[14–18] found a more general description of CFL envelopes by means of a bell-shaped function. While the overall asymmetry and the overall non-linearity in the CFL diagram for a composite were considered in these attempts, a change in shape of CFL envelope with increasing constant value of life was not explicitly taken into account. These pioneering attempts thus aroused a concern of explicit consideration of the change in shape of CFL envelope with increasing value of life, in addition to ease of construction of the CFL diagrams for composites. With these views in mind, Kawai[24] and Kawai and Koizumi[25] have recently proposed a new and efficient method, called the anisomorphic CFL diagram approach, for describing the asymmetric and non-linear CFL diagram for a given composite laminate using only the *S–N* relationship for a particular stress ratio and the static strengths in tension and compression. The use of fatigue data for the particular stress ratio, called the critical stress ratio, that is given by the ratio of compressive strength to tensile strength is the distinguishing feature of this method. The anisomorphic CFL diagram approach was shown to be applicable to fiber-dominated fatigue life prediction of multidirectional CFRP laminates in different lay-ups.[25] Vassilopoulos et al.[26] have also attempted to develop a different CFL diagram that is drawn in the stress ratio versus alternating stress amplitude plane, instead of the mean stress versus alternating stress amplitude plane, by means of piecewise-defined functions. These modern attempts are driving establishment of engineering fatigue life prediction methods for composites. A little more detailed review that has recently been published in Kawai [12] would supplement the above short exploration of latest development of engineering methods for describing the overall non-linear CFL diagrams for composites.

These CFL models for composites[23–26] have been developed with a view to apply them for their engineering fatigue analysis on a laminate level. By contrast, fatigue life prediction of composite laminates on a ply-by-ply basis is another rational approach to evaluation of their *S–N* relationships.[27,28] For the fatigue failure analysis of multidirectional composite laminates on a ply level, it is a prerequisite to develop a model for predicting the fatigue behavior of a unidirectional composite ply under various modes of on-axis and off-axis fatigue loading conditions. A number of different attempts have been made to model the on-axis and off-axis fatigue behaviors of unidirectional composites. For example, Hashin and Rotem[29] and Sims and Brogdon[30] developed fatigue failure criteria by replacing the principal strengths in underlying static failure criteria with the principal fatigue strengths that depend not only on the number of cycles but also on the parameters that characterize fatigue loading. Ellyin and El-Kadi[31] proposed an off-axis fatigue life prediction method on the basis of a master *S–N* relationship that is determined by means of elastic strain energy. Awerbuch and Hahn[32] confirmed that the maximum fatigue stress normalized using tensile strength becomes an effective measure for off-axis fatigue data analysis of unidirectional graphite/epoxy composites. Fawaz and Ellyin[33] developed a stress-based approach to establishing the master *S–N* relationship that is independent of stress ratio as well as fiber orientation. Kawai et al.[34,35] proved that the fatigue strength ratio can be defined theoretically in terms of a non-dimensional effective stress, and successfully applied it to identification

of a master S–N relationship for the off-axis fatigue behaviors of unidirectional carbon/epoxy composites. A more general form of the non-dimensional effective stress was also developed,[10] and it was shown to be useful for identifying the master S–N relationship that is independent of stress ratio as well as fiber orientation. While these methods are attractive, however, neither identification of analytical expressions of the principal fatigue strength functions that depend on the mode of fatigue loading nor identification of a unified measure to define a master S–N curve into which all the factors of fatigue loading are lumped is straightforward because of the complexity of the loading mode dependence of fatigue failure of unidirectional composites.

A ply-level CFL diagram approach for a unidirectional composite allows bypassing the difficulties involved by the methods mentioned above. If the CFL diagrams for a unidirectional composite in the principal directions of material anisotropy are available, they allow not only non-analytically predicting the principal fatigue strengths that depend on the mode of fatigue loading, but also predicting the off-axis CFL diagrams for unidirectional CFRP laminates in any fiber orientations over the whole range of mean stress without identifying a master S–N curve for all possible modes of loading. This suggests that we can develop a multiaxial fatigue model on the basis of the principal CFL diagrams. To the best of the authors' knowledge, however, the only information available about an attempt that is consistent with the line mentioned above can be found in the experimental results reported by Philippidis and Vassilopoulos.[36,37] They performed constant amplitude fatigue tests on coupon specimens that were cut out from a multidirectional glass fiber reinforced plastic (GFRP) laminate $[0/(\pm 45)_2/0]_T$ panel in different orientations and examined the effect of loading direction on the CFL diagram for the multidirectional GFRP laminate. The experimental results from this study showed that the CFL diagram for the GFRP laminate significantly depends on the direction of fatigue loading, and the resulting CFL diagrams consist of very complicated shapes of CFL envelopes that depend on off-axis fiber orientation. These observations appear to show that a piecewise linear approximation can only be applied to describe the complicated shapes of the CFL envelopes, which are non-linear overall, for the multidirectional GFRP laminate under off-axis fatigue loading conditions. At this stage in the understanding of the off-axis CFL diagrams for orthotropic fiber composites, however, it is not clear whether the mean stress sensitivity in the off-axis fatigue failure of the multidirectional GFRP laminate is similar to that in the off-axis fatigue failure of a unidirectional CFRP laminate. To make it clear, therefore, we need fundamental and systematic experiments to identify the full shapes of off-axis CFL diagrams for a unidirectional CFRP laminate in different fiber orientations. For prediction of the fatigue lives of composite laminates on a ply-by-ply basis, moreover, we need a theoretical study to establish a framework for efficiently and accurately describing the overall non-linear shape of off-axis CFL diagram for a unidirectional composite that depends on fiber orientation. In this context, it is a challenging and interesting attempt to develop a highly flexible framework for that purpose taking full advantage of the anisomorphic CFL diagram approach. These are the prerequisites of establishing a CFL based multiaxial fatigue model for multidirectional composite laminates.

In this study, the full shapes of the off-axis CFL diagrams for a unidirectional carbon/epoxy laminate in different fiber orientations are examined, and the effect of fiber orientation on the shape of off-axis CFL diagram is observed. On the basis of these experimental results, moreover, a failure-mode based anisomorphic CFL diagram that allows accurately and efficiently describing the off-axis CFL diagrams for the unidirectional CFRP laminate is developed. First, constant amplitude fatigue tests at different stress ratios are performed on coupon specimens in different fiber orientations, respectively, in order to examine the mean stress sensitivity and the fiber orientation dependence of the off-axis fatigue behavior of the unidirectional CFRP laminate. The off-axis CFL diagrams for different fiber orientations are identified on the basis of the fatigue data obtained. They are compared to observe the effect of fiber orientation on the shape of the off-axis CFL diagram for the unidirectional CFRP laminate. Then, a most general member of the family of anisomorphic CFL diagram is developed that takes into account different sensitivities to the modes of fatigue failure under different modes of fatigue loading and thus reflects the physical mechanisms of fatigue failure indirectly. It is demonstrated that the generalized anisomorphic CFL diagram allows accommodating itself to the highly non-linear and asymmetric off-axis CFL diagrams for the unidirectional CFRP laminate, and thus, it can be successfully applied to accurate description of the off-axis CFL diagram for the unidirectional CFRP laminate, regardless of fiber orientation. Since the number of test data for the same loading conditions is limited, we attempt to draw only suggestive conclusions from the experimental results concerning the off-axis fatigue behavior and the associated off-axis CFL diagram for the unidirectional laminate. Accordingly, only a potential usefulness of the generalized anisomorphic CFL diagram approach proposed in this study is proved.

Experiment

Material and specimens

The material used in this study was a unidirectional composite laminate fabricated from T700S/2592 carbon/epoxy prepreg tapes (P3252-20, TORAY). The lay-up of virgin laminates is $[0]_{16}$, and they were cured in an autoclave. The thickness of as-received laminates was about 3.1 mm.

Specimens were cut into parallel-sided coupons in six fiber orientations ($\theta = 0^\circ$, 10°, 15°, 30°, 45°, and 90°). The off-axis angle θ indicates the fiber direction (1-axis) relative to the longitudinal direction (x-axis) of a coupon specimen. Two kinds of coupon specimens in different nominal dimensions were utilized in this study, as shown in Figure 1. For the static tension and tension–tension (T–T) fatigue tests in which only tensile load is applied to specimens, long specimens based on the testing standards JIS K7073[38] and JIS K7083[39] were employed; the dimensions of long specimens were gage length $L_G = 100$ mm and width $W = 20$ mm. The specimen width (W) was 10 mm for the fiber direction ($\theta = 0^\circ$) and 20 mm for the other fiber orientations ($0^\circ < \theta \leq 90^\circ$). In the static compression tests and the compression–compression (C–C) and tension–compression (T–C) fatigue tests, on the other hand, short specimens were used to reduce a risk of buckling under compressive load; the dimensions were gage length $L_G = 10$ mm and width $W = 10$ mm. The nominal dimensions of short specimens were determined on the basis of the testing standard JIS K7076[40] and the report of Haberle and Matthews[41] that discussed the compression test methods suitable for composite laminates. Rectangular-shaped aluminum alloy tabs were glued on both ends of specimens with epoxy adhesive in order to protect their gripped portions.

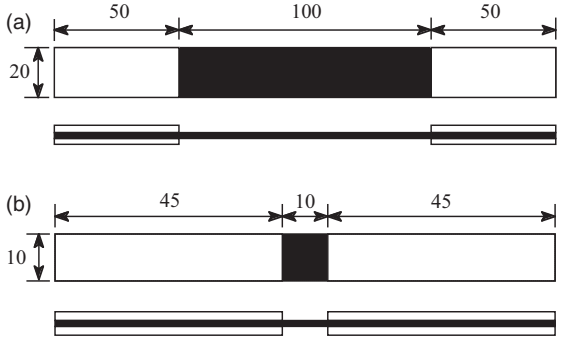

Figure 1. Specimen geometry (dimension in mm): (a) tensile and (b) compressive.

Test procedure

Load-controlled off-axis fatigue tests were performed at room temperature (~23 °C). Fatigue load was applied in a sinusoidal waveform with a frequency of 5 Hz. Specimens were fatigue tested for up to 10^6 cycles. Constant amplitude fatigue tests were performed, in principle, at five different stress ratios $R = 0.1$, 0.5, 2, 10, and χ for each of the fiber orientations, where $\chi \in (-\infty, 0)$ represents the critical stress ratio defined as the ratio of compressive strength σ_C (<0) to tensile strength σ_T (>0); i.e.

$$\chi = \frac{\sigma_C}{\sigma_T} \tag{1}$$

To examine the mean stress sensitivity in fatigue in the vicinity of the critical stress ratio in a little more detail, additional fatigue tests were conducted under the following conditions: $R = -1$ ($\theta = 0^\circ$, 45°, and 90°); $R = -3$ ($\theta = 10^\circ$, 15°, and 30°); and $R = -10$ ($\theta = 45^\circ$ and 90°). Anti-buckling guide fixtures were not used for T–C and C–C fatigue tests in this study since short specimens were used to reduce possible buckling of specimens under compressive loading conditions. Apparently, no clear indication of buckling was seen in short specimens that failed under static and fatigue loading conditions. The fatigue test matrix is presented in Table 1 with the number of specimens used for each loading condition.

Static tension and compression tests were performed on the coupon specimens at room temperature to determine the stress levels for fatigue testing. The static tests were carried out at a constant nominal strain rate of 1.0%/min, following the testing standard JIS K7073.[38] The off-axis static and fatigue tests were conducted on a servo-hydraulic test machine (MTS 810 Test Star). No attempt was made to control the moisture content of the specimens.

Table 1. Fatigue test matrix with the number of specimens allocated to each loading condition.

	R							
θ (°)	0.5	0.1	χ	−1	−3	−10	10	2
0	3	5	6	5	0	0	4	2
10	4	5	6	0	4	0	6	2
15	5	5	6	0	4	0	4	3
30	6	5	5	0	4	0	4	3
45	4	5	8	3	0	5	4	2
90	3	7	11	2	0	8	3	2

Experimental results and discussion

Mean stress dependence of on-axis and off-axis S–N relationships

The overall feature of the shape of the S–N relationship for the unidirectional CFRP laminate under off-axis fatigue loading and the effect of mean stress are observed on the basis of the representative fatigue test results obtained. The off-axis S–N relationships for the other fiber orientations are presented later in the comparison with prediction using an extended anisomorphic CFL diagram approach proposed in this study.

The fatigue data for the fiber orientations $\theta = 0°$, $45°$, and $90°$ are presented in Figures 2(a) to (c), respectively, as plots of the maximum fatigue stress level, σ_{max} for T–T loading and T–C loading and $|\sigma_{min}|$ for C–C loading, against the number of reversals to failure $2N_f$ on the linear and log scales. Each of these figures includes the data from the T–T, C–C, and T–C fatigue tests at the representative stress ratios $R = 0.1$, 10, and χ. The ultimate tensile and compressive strengths are plotted as the ordinates at $N_f = 0.5$ in these figures. The dashed lines in these figures indicate the approximate curves fitted to the fatigue data for respective stress ratios, helping us to understand the approximate shapes of the S–N relationships in different fatigue loading conditions.

It is seen that the dashed line fitted to the fatigue data extrapolates back to the tensile strength in the case of T–T fatigue loading ($R = 0.1$), and to the compressive strength in the case of C–C fatigue loading ($R = 10$), regardless of fiber orientation. The S–N relationship associated with the critical stress ratio χ can approximately be described by means of a curve that extrapolates back to the larger level of static strength; namely to the tensile strength if $\theta = 0°$ and to the compressive strength if $\theta = 45°$ and $90°$. Note that the tensile strength of the unidirectional CFRP laminate is larger than the compressive strength under static loading in the fiber direction ($\theta = 0°$), while the order turns opposite under static loading in the $45°$ and $90°$ directions.[42] Correspondingly, it is suggested that the value of the off-axis critical stress ratio largely changes depending on the fiber orientation of the specimen. The off-axis tensile and compressive strengths and the

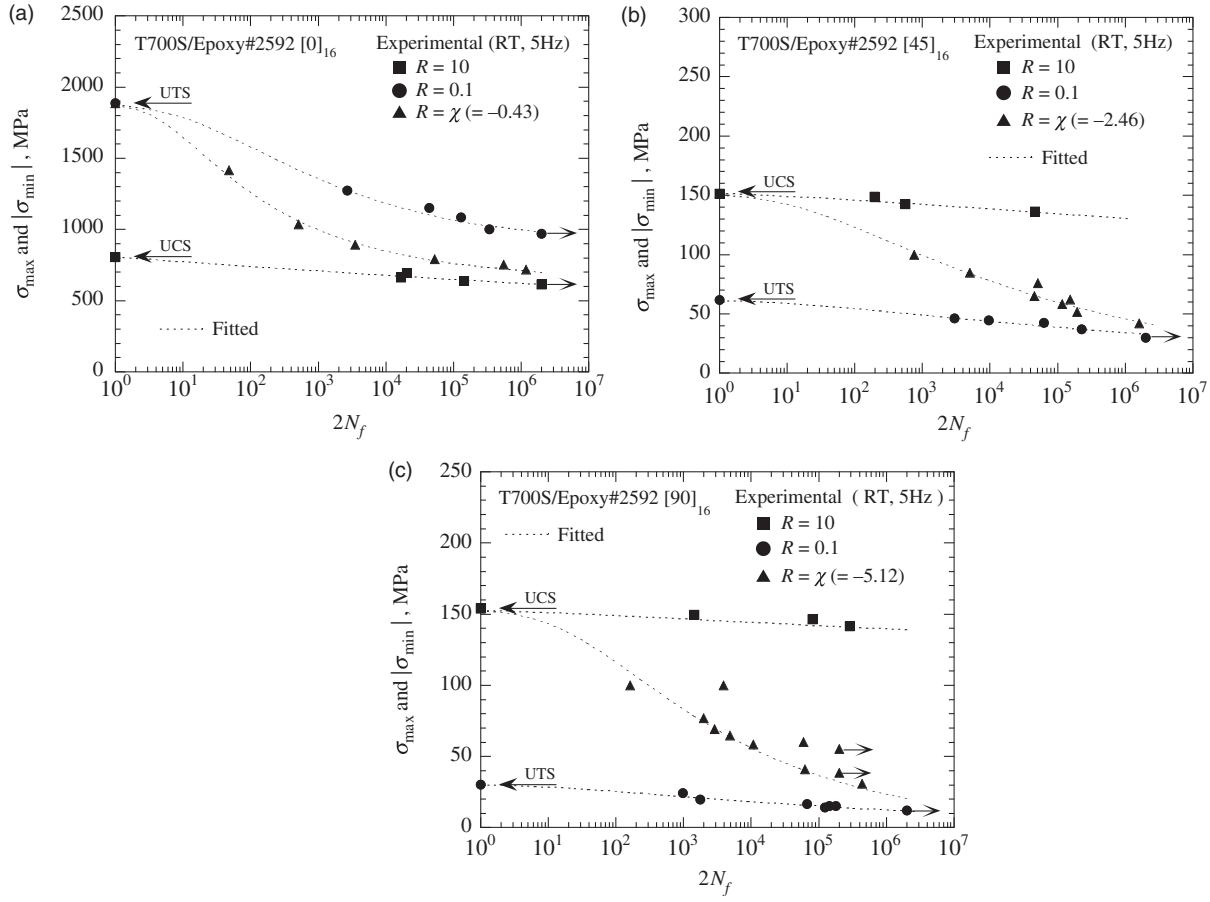

Figure 2. Off-axis S–N relationships for different stress ratios: (a) $\theta = 0°$; (b) $\theta = 45°$; and (c) $\theta = 90°$.

off-axis critical stress ratios of the unidirectional CFRP laminate are presented in Table 2.

For each of these fiber orientations, the S–N relationship for $R = \chi$ exhibits a larger gradient than the S–N relationships for $R = 0.1$ and 10. Moreover, the fatigue data $R = \chi$ are distributed between those for $R = 0.1$ and 10. These features were observed for all the other fiber orientations tested in this study as well. These results show that fatigue damage accumulates more rapidly under T–C fatigue loading near the critical stress ratio than under T–T or C–C fatigue loading, suggesting that fatigue damage is developed more significantly by a larger change in alternating stress. In fact, the most rapid degradation under T–C fatigue loading at the critical stress ratio has been observed in quasi-isotropic and cross-ply CFRP laminates.[25] The endurance limits cannot be identified in the tested range, regardless of stress ratio and fiber orientation.

Incidentally, the typical modes of macroscopic fatigue failure for different stress ratios and fiber orientations can obviously be classified into two groups: a mode of tensile failure (T) and a mode of compressive failure (C). The compressive failure can further be categorized according to a dominant failure mode: a kink mode (C_K); an in-plane shear mode (C_{IS}); and an out-of-plane shear mode (C_{OS}). These observations are summarized in Table 3.

Table 2. Off-axis tensile and compressive strengths of the unidirectional T700S/2592 carbon/epoxy laminate at room temperature.

Off-axis angle, θ (°)	σ_T (MPa)	σ_C (MPa)	$\chi = \sigma_C/\sigma_T$
0	1887.1	−806.5	−0.43
10	343.0	−313.0	−0.91
15	210.9	−234.0	−1.11
30	101.1	−163.6	−1.62
45	61.6	−151.6	−2.46
90	30.1	−154.0	−5.12

Application of the two-segment anisomorphic CFL model

The off-axis CFL diagrams for all the fiber orientations examined in this study are shown in Figure 3(a) to (f), respectively. The symbols in these figures indicate the fatigue strengths for constant values of life $N_f = 10^x$ ($x = 1$, 2, 3, 4, 5, and 6), and they were evaluated using the approximate S–N curves fitted to the fatigue data obtained. The dashed lines indicate the predictions using the two-segment anisomorphic CFL diagram approach.[24,25] As mentioned above, the off-axis critical stress ratios $\chi(\theta)$ in different fiber orientations are presented in Table 2. From this table, it is observed that $\chi(\theta) < -1$ in the range $15^\circ \le \theta \le 90^\circ$ since the compressive strength becomes larger than the tensile strength in that range. The asymmetry in off-axis static strength in tension and compression can be visualized by means of the profile of anisomorphic CFL diagram that consists of segments given by $\sigma_a + \sigma_m = \sigma_T$ and $\sigma_a - \sigma_m = \sigma_C$, respectively. It demonstrates that the anisomorphic CFL diagram for off-axis fatigue loading in the direction inclined at any off-axis angle in the range $15^\circ \le \theta \le 90^\circ$ has a peak in the second quadrant in the alternating stress versus mean stress plane.

More detailed observation about the CFL diagram in each fiber orientation is attempted. From Figure 3(a), it is observed that the longitudinal CFL envelopes for loading in the fiber direction ($\theta = 0^\circ$) have their peaks in the first quadrant, and incline to the right of the alternating stress axis, because of a larger static strength in tension. The peaks of CFL envelopes appear under fatigue loading at the critical stress ratio over the range of fatigue life tested in this study. In Figure 3(a), for $\theta = 0^\circ$, it is observed that the two-segment anisomorphic CFL diagram agrees well

Table 3. Macroscopic fatigue failure modes observed for different loading conditions.

	R							
θ (°)	0.5	0.1	χ	−1	−3	−10	10	2
0	T	T	T, C_K, C_{IS}	C_K, C_{IS}	–	–	C_K, C_{IS}	C_K, C_{IS}
10	T	T	T, C_K, C_{IS}	–	C_K, C_{IS}	–	C_K, C_{IS}	C_K
15	T	T	T, C_K, C_{IS}	–	C_K, C_{IS}	–	C_K	C_K
30	T	T	T, C_{IS}	–	T, C_K, C_{IS}	–	C_K	C_{IS}, C_{OS}
45	T	T	T	T	–	T, C_{OS}	C_{OS}	C_{OS}
90	T	T	T	T	–	T, C_{OS}	C_{OS}	C_{OS}

T: tensile failure; C: compressive failure; C_K: kink failure; C_{IS}: in-plane shear failure; C_{OS}: out-of-plane shear failure; –: NA.

with the experimental CFL diagram. The agreement between the theoretical and experimental CFL diagrams for $\theta = 0^\circ$ reveals that the shape of the longitudinal CFL envelope gradually changes with increasing constant value of life, and the transition in shape from a straight line to a parabola that is assumed in the two-segment anisomorphic CFL diagram is a good approximation to the change in shape of the longitudinal CFL envelope observed by experiment. Note that the experimental CFL data for $R = 0.1$ and 10 were not used in constructing the two-segment anisomorphic CFL diagrams not only for $\theta = 0^\circ$ but also for the other off-axis angles.

The off-axis CFL diagrams for $\theta = 10^\circ$ and 15° that are shown in Figure 3(b) and (c), respectively, have their peaks close to the alternating stress axis, in the first quadrant for the case $\theta = 10^\circ$ and in the second quadrant for the case $\theta = 15^\circ$. However, the CFL data are distributed asymmetrically. The profile of the off-axis CFL diagram inclines only slightly to the right of the alternating stress axis for the case $\theta = 10^\circ$ and to the left for the case $\theta = 15^\circ$. The approximately symmetrical profiles of the CFL diagrams for these fiber orientations is due to almost equal magnitude in off-axis static strength in tension and compression. By contrast, the off-axis CFL envelopes for different constant values of life are asymmetric, indicating that the mean stress sensitivity in fatigue differs between under tension-dominated off-axis fatigue loading and under compression-dominated off-axis fatigue loading. It should also be noted that the CFL envelopes have peaks under fatigue loading at the critical stress ratio in the low cycle range up to about 10^3 cycles, but they are apt to have peaks at a stress ratio between $R = -3$ and $R = 10$ in the high cycle range beyond 10^3 cycles. Comparing with the prediction using the two-segment

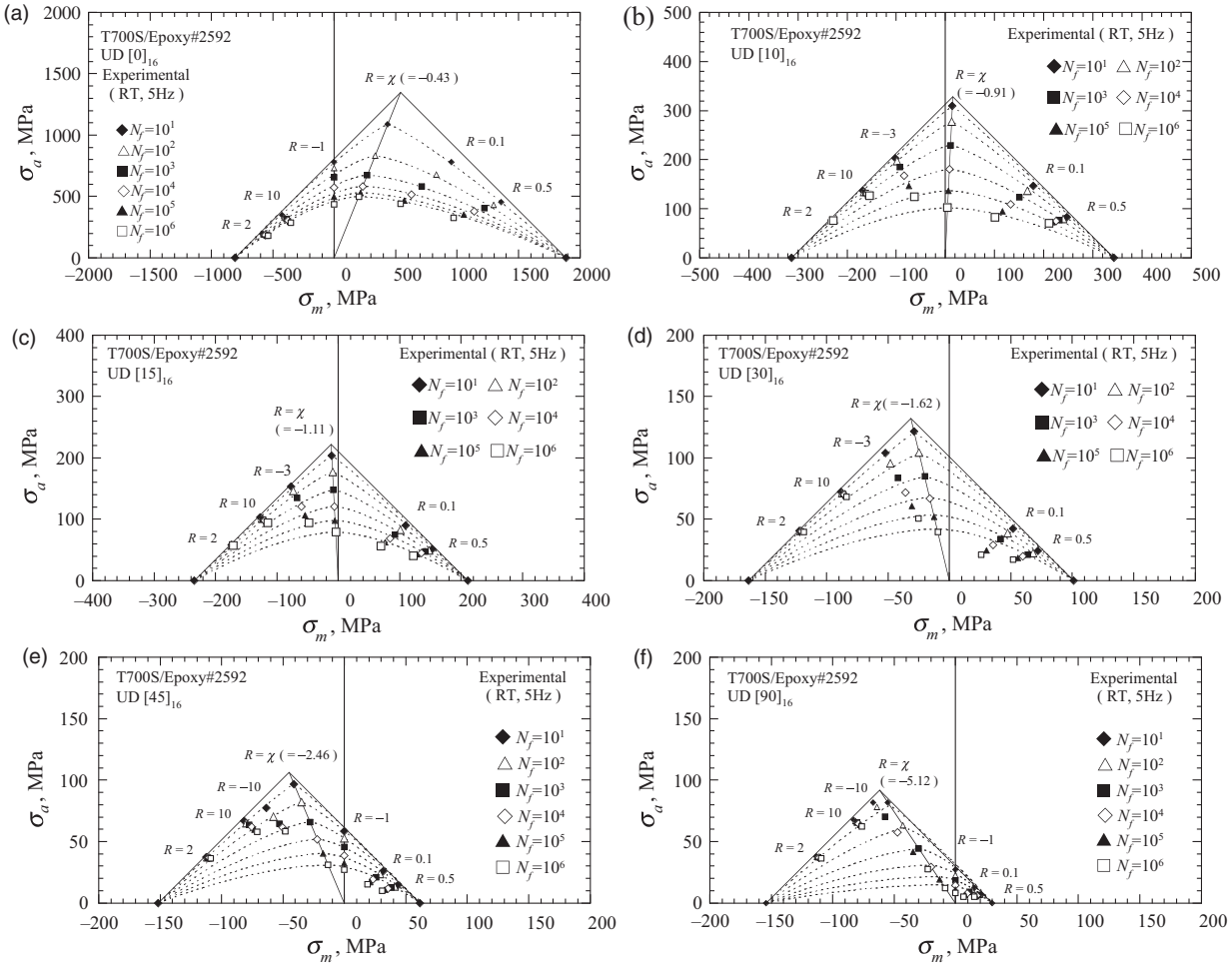

Figure 3. Off-axis CFL diagrams in different fiber orientations and comparison with those predicted using the two-segment anisomorphic CFL diagram approach: (a) $\theta = 0^\circ$; (b) $\theta = 10^\circ$; (c) $\theta = 15^\circ$; (d) $\theta = 30^\circ$; (e) $\theta = 45^\circ$; and (f) $\theta = 90^\circ$.

anisomorphic CFL diagram approach, we can see very good agreements between the predicted and observed CFL envelopes in the right segment associated with T–T and tension-dominated T–C fatigue loading conditions. However, the agreement between theory and experiment in the left segment associated with C–C and compression-dominated T–C fatigue loading conditions is worse than that in the right segment. More specifically, the two-segment anisomorphic CFL model slightly overestimates the mean stress dependence of the off-axis fatigue behavior under compression-dominated fatigue loading conditions.

The CFL diagrams for larger off-axis angles $\theta = 30$–90° incline more significantly to the left of the alternating stress axis, as can be observed from Figure 3(d) to (f). The remarkable asymmetry in the shape in these CFL diagrams reflects a significant difference between the fatigue strengths under tension-dominated and compression-dominated off-axis fatigue loading conditions, and it also suggests that a significant change in mean stress sensitivity in fatigue occurs in between. The value of stress ratio at which the peak of a CFL envelope appears changes earlier in life in the low cycle range as the off-axis angle increases, and thus, the overall CFL diagram inclines more significantly to the left of the alternating stress axis. The two-segment anisomorphic CFL diagrams for these fiber orientations deviate from the experimental CFL diagrams both in the right and left segments associated with tension-dominated and compression-dominated fatigue loading conditions, respectively; it appears that the deviation is more significant in the left segment associated with C–C fatigue loading.

These observations suggest that while it is applicable to the unidirectional CFRP laminate for the prediction of the fiber-dominated fatigue behavior in the fiber direction ($\theta = 0^\circ$), the assumption of relying on only the fatigue data for the critical stress ratio to construct the two-segment anisomorphic CFL diagram over the whole range of mean stress becomes less valid as the off-axis angle of a specimen increases. The tendency for the two-segment anisomorphic CFL diagram to lose its descriptive accuracy with increasing fiber orientation is more significant in the left segment associated with C–C fatigue loading. The strength and limitation of the two-segment anisomorphic CFL diagram are reflected by the S–N relationships predicted. It was confirmed that the agreement between the predicted and observed S–N relationships is reasonable for the on-axis fatigue loading in the fiber direction $\theta = 0^\circ$, but not satisfactory for the off-axis fatigue loading in the direction $\theta = 45^\circ$.

In the previous studies,[24,25] we observed that the two-segment anisomorphic CFL diagram approach is applicable to quasi-isotropic and cross-ply CFRP laminates in the prediction of lives under fatigue loading in one of their fiber directions. These previous observations along with the present results for $\theta = 0^\circ$ suggest that the two-segment anisomorphic CFL diagram can successfully be applied to prediction of the fiber-dominated fatigue lives of most CFRP laminates with reasonable accuracy.

Application of the three-segment anisomorphic CFL model

Figure 4(a) to (f) shows the three-segment anisomorphic CFL diagrams[43] applied to the off-axis fatigue data for different fiber orientations, $\theta = 0^\circ$, 10°, 15°, 30°, 45°, and 90°, respectively. A transitional segment $[\chi_S, \chi]$ was introduced to the left of the critical line. The value of the sub-critical stress ratio was assumed as $\chi_S = -\infty$. The fatigue strengths for constant values of life under fatigue loading at the sub-critical stress ratio $\chi_S = -\infty$ were evaluated by linear extrapolation of the linear CFL envelopes on the C–C segment $[\sigma_C, \sigma_m^{(R=10)}]$. The need for the additional reference fatigue data for the sub-critical stress ratio slightly impairs the simplicity of the anisomorphic CFL diagram approach. In order to relax the requirement, the piecewise linear CFL envelopes on the three segments are assumed. Note that the piecewise linear CFL diagram is a particular case of the three-segment anisomorphic CFL diagram with $k_T = k_C = 0$, and it still features the asymmetry and the overall non-linearity of CFL envelopes that are determined by the critical and sub-critical stress ratios.

From Figure 4, it is observed that the accuracy of prediction of the overall shapes of off-axis CFL envelopes using the three-segment anisomorphic CFL diagram is greatly enhanced, regardless of fiber orientation. The improvement of predictive accuracy for compression-dominated fatigue loading is significant. This proves that the transitional segment helps accommodating the three-segment anisomorphic CFL diagram to the marked change in mean stress sensitivity in off-axis fatigue. It can thus be confirmed that the use of fatigue data for the sub-critical stress ratio $R = \chi_S$ along with those for the critical stress ratio $R = \chi$ greatly contributes to enhancement of predictive accuracy of the anisomorphic CFL diagram approach. Consequently, it is suggested that the three-segment anisomorphic CFL diagram can be used for describing the non-linear and asymmetric off-axis CFL diagram for the unidirectional CFRP laminate over the whole range of mean stress, regardless of fiber orientation. The observation above and that in the previous studies[43] thus prove that the three-segment anisomorphic CFL diagram has the potential of adequately describing the overall non-linear CFL diagrams associated

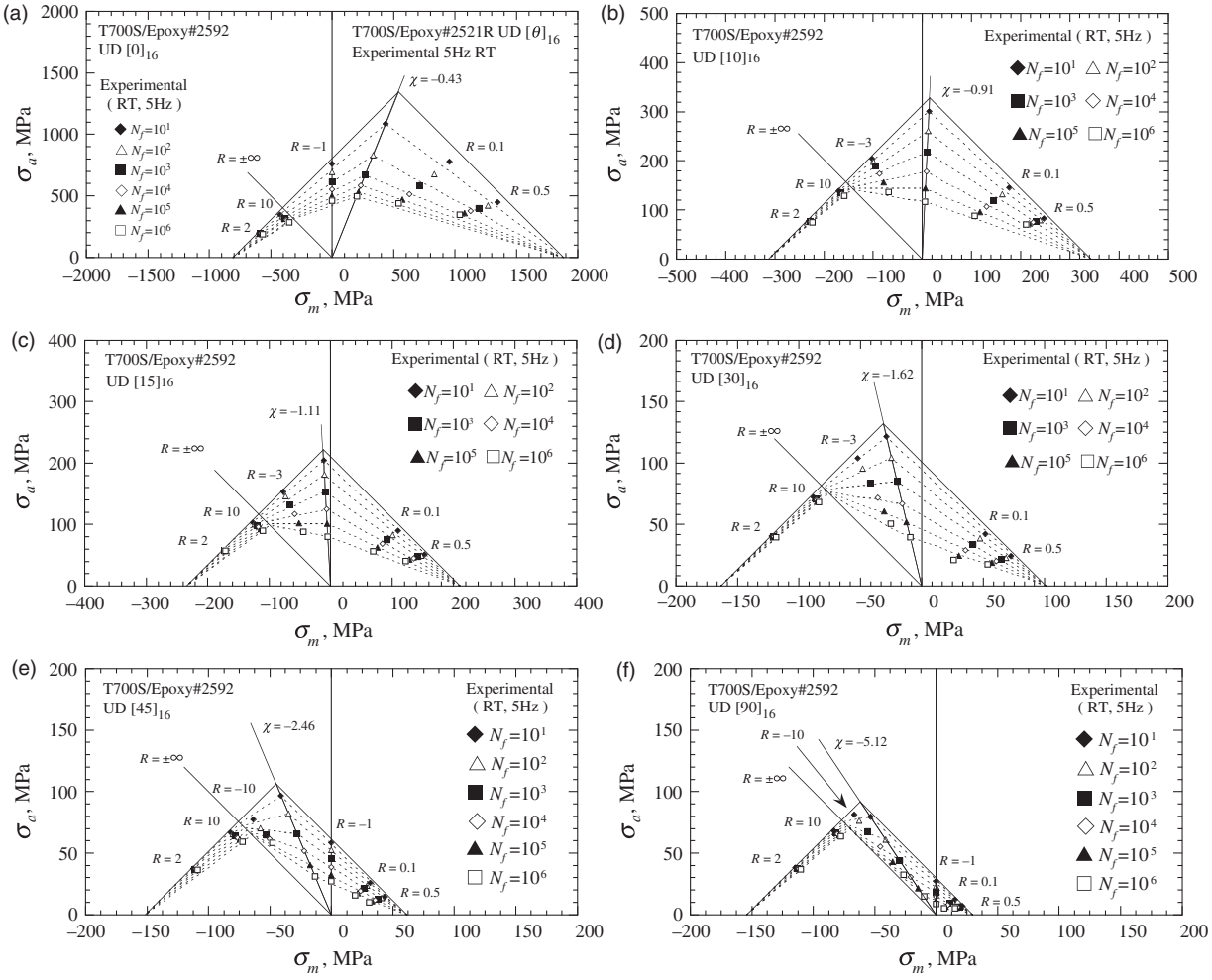

Figure 4. Off-axis CFL diagrams predicted using the three-segment anisomorphic CFL diagram approach: (a) $\theta = 0^\circ$; (b) $\theta = 10^\circ$; (c) $\theta = 15^\circ$; (d) $\theta = 30^\circ$; (e) $\theta = 45^\circ$; and (f) $\theta = 90^\circ$.

with a matrix-dominated fatigue behavior as well as with a fiber-dominated fatigue behavior of composites.

It is interesting to observe how close the CFL envelopes for stress ratios near the critical and sub-critical values are distributed. The experimental results show a significant difference between the densities of packing of CFL envelope near the critical and sub-critical stress ratios. The CFL envelopes are more sparsely nested at the critical stress ratio, corresponding to a larger gradient of the *S–N* relationship under fatigue loading at the critical stress ratio. By contrast, the CFL envelopes for fatigue loading near the sub-critical stress ratio are more densely nested because of a very small gradient of the *S–N* relationship under C–C fatigue loading. This suggests that the mean stress sensitivity in the off-axis fatigue behavior of the unidirectional CFRP laminate significantly changes in the transitional segment.

The exact shape of CFL envelope on the transitional segment was not identified. For the sake of simplicity, it was assumed to be linear instead in this study. Some fatigue data were obtained for stress ratios that belong to the transitional segment, and they are plotted in Figure 4. It is seen that those CFL data points almost fall on the assumed linear CFL envelopes, indicated by dashed lines, on the transitional segment. This agreement justifies in part the assumption of linear interpolation on the transitional segment.

While the linear CFL envelopes assumed in this application tend to result in conservative predictions, the *S–N* relationships predicted using the three-segment CFL diagram approach reasonably agreed with the experimental results for different stress ratios, regardless of fiber orientation. These observations prove that the three-segment CFL diagram is furnished with an enhanced capability to describe the non-linear and

asymmetric off-axis CFL diagrams for the unidirectional composite.

Fiber orientation dependence of off-axis CFL diagram

The comparisons between the profiles of the off-axis CFL diagrams for all the fiber orientations are shown in Figure 5. From this figure, it is observed that the CFL diagram for loading in the fiber direction is much larger than the CFL diagrams for loading in the other off-axis directions, and the size of CFL diagram significantly decreases by only a small angle of deviation from the fiber direction. Such a large change in the size of the off-axis CFL diagram reflects a marked reduction in off-axis static strength with increasing off-axis angle. These profiles of off-axis CFL envelopes visualize the fiber orientation dependence of off-axis fatigue load bearing capability of unidirectional composites. Obviously, the identification of nested off-axis CFL envelopes wrapped in the profile allows us to quickly quantify the off-axis fatigue strength of a unidirectional composite for a given fiber orientation and for a given number of cycles.

A generalized anisomorphic CFL diagram for unidirectional composites

Non-classical classification of fatigue loading

The slope of S–N curve for a composite material is usually larger in T–C loading than in T–T or C–C loading, regardless of the stacking configuration of its laminated structure,[4,25,44–46] for example, as can be observed from Figure 2 for the case of the unidirectional composite tested in this study. This fact suggests that T–C loading is more damaging than T–T or C–C loading.

Gamstedt and Sjogren[47] have identified the major mechanism of higher sensitivity to fatigue of composites in T–C loading. It was explained by the opening of large debond cracks at the matrix–fiber interface in compressive loading. The local instability and buckling

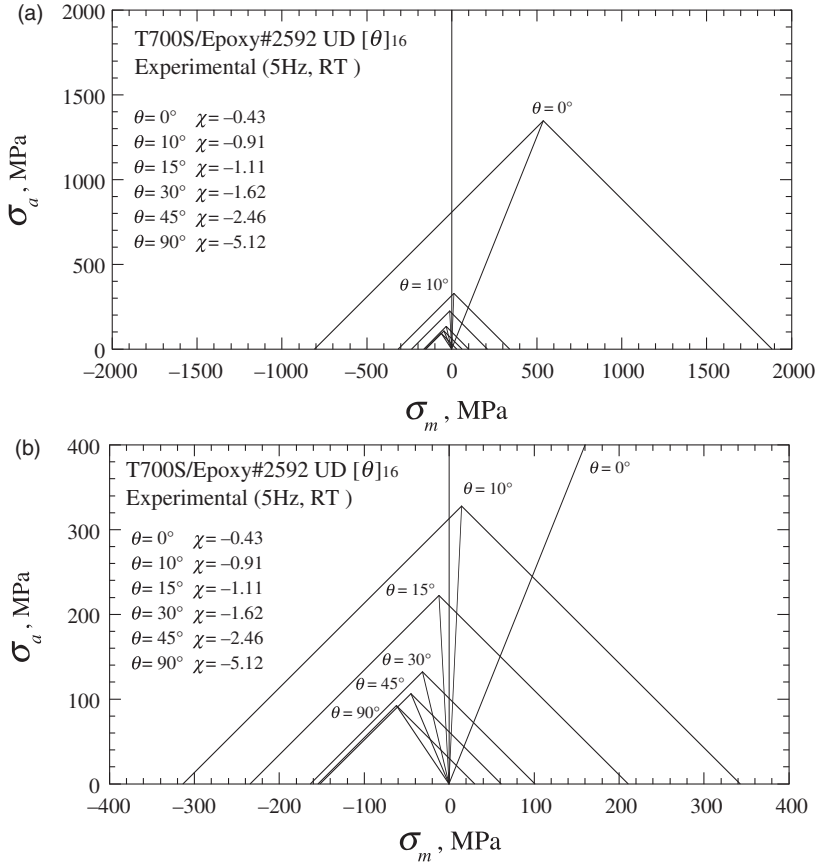

Figure 5. Comparison of the profiles of off-axis CFL diagrams in different fiber orientations: (a) common scale and (b) magnified scale.

of load bearing fibers are highly susceptible to the transverse cracks in plies and the local interlaminar delamination that are developed during T–C loading.[4] El-Kadi and Ellyin[8] have pointed out an unequal effect of tensile and compressive stresses during T–C cycling on the overall deterioration of composites. The fatigue failure modes in T–T and C–C loading are different,[48] and they are often similar to those in static tension and compression.

These observations suggest the necessity of distinguishing between the fatigue behaviors under T–T, C–C, and T–C fatigue loading. T–C loading may further be classified into two cases: a T–C loading case that is apt to cause tension-dominated fatigue failure and a T–C loading case that is apt to cause compression-dominated fatigue failure. Therefore, it is natural to classify the waveform or stress ratio of fatigue loading into four groups. Figure 6(a) schematically illustrates an example of the four divisions of the range of stress ratio for the case of materials with equal strength in tension and compression. The four segments are defined by the stress ratios $R=0$, -1, and ∞. This is a classical view of distinguishing the fatigue behavior of a material on the basis of mean stress sensitivity.

Most composites, however, exhibit different strengths in tension and compression.[25,42] In those cases, Figure 6(a) should be modified as presented in Figure 6(b) or (c). If tensile strength is larger than compressive strength, the margin to static failure is larger in tension, and thus the value of mean stress of equal distance from the tensile and compressive strengths deviates from zero to a positive number, as illustrated in Figure 6(b). If compressive strength is larger, by contrast, the margin to static failure is larger in compression, and accordingly, the neutral level of mean stress deviates to a negative value, as illustrated in Figure 6(c). Therefore, it is reasonable to divide T–C loading into tension-dominated T–C loading and compression-dominated T–C loading by assuming a particular stress ratio at which mean stress always has a value of equal distance from the tensile and compressive strengths. The particular stress ratio is identified with the critical stress ratio that is assumed in the anisomorphic CFL diagram approach.[24,25] Consequently, the non-classical classification of mean stress sensitivity in fatigue, which is illustrated in Figure 6(b) and (c), suggests two-sided modification of the two-segment anisomorphic CFL diagram into a four-segment version. The four-segmentation of the anisomorphic CFL diagram removes the procedure of judging which segment of the two-segment anisomorphic CFL diagram should be modified that is encountered when applying the three-segment anisomorphic CFL diagram. It also allows us to feel secure about the accuracy of prediction since it obviously enhances the descriptive capability. It is a welcome feature as well that the four-segmentation provides a failure-mode based framework for modeling the fatigue of composites.

A failure-mode based four-segment anisomorphic CFL model

The non-classical view of the mean stress sensitivity in fatigue of composites suggests formulating a four-segment version of the anisomorphic CFL diagram that allows more accurately describing the highly non-linear and asymmetric off-axis CFL diagrams for unidirectional composites in different fiber orientations.

In the general four-segment anisomorphic CFL diagram, the right and left transitional segments are defined as $[\chi, \chi_R] = \{R : -\infty < \chi \le R \le \chi_R \le 0\}$ and $[\chi_L, \chi] = \{R : -\infty \le \chi_L \le R \le \chi < 0\}$, respectively, using two auxiliary stress ratios χ_L and χ_R in conjunction with the critical stress ratio χ. The right and left auxiliary stress ratios χ_R and χ_L are determined so as to satisfy the condition $-\infty \le \chi_L \le \chi \le \chi_R \le 0$. The total interval of mean stress $[\sigma_C, \sigma_T]$ is thus separated into four sub-intervals: I. $[\sigma_m^{(\chi_R)}, \sigma_T]$; II. $[\sigma_m^{(\chi)}, \sigma_m^{(\chi_R)}]$; III. $[\sigma_m^{(\chi_L)}, \sigma_m^{(\chi)}]$; and IV. $[\sigma_C, \sigma_m^{(\chi_L)}]$. The CFL envelopes on these sub-intervals are described by means of the following piecewise-defined functions:

(I) tension-dominated zone $(\sigma_m^{(\chi_R)} \le \sigma_m \le \sigma_T)$

$$-\frac{\sigma_a - \sigma_a^{(\chi_R)}}{\sigma_a^{(\chi_R)}} = \left(\frac{\sigma_m - \sigma_m^{(\chi_R)}}{\sigma_T - \sigma_m^{(\chi_R)}}\right)^{2-\psi_{\chi_R}^{k_T}} \tag{2}$$

(II) right transitional zone $\left(\sigma_m^{(\chi)} \le \sigma_m < \sigma_m^{(\chi_R)}\right)$

$$-\frac{\sigma_a - \sigma_a^{(\chi_R)}}{\sigma_a^{(\chi_R)} - \sigma_a^{(\chi)}} = \frac{\sigma_m - \sigma_m^{(\chi_R)}}{\sigma_m^{(\chi)} - \sigma_m^{(\chi_R)}} \tag{3}$$

(III) left transitional zone $\left(\sigma_m^{(\chi_L)} \le \sigma_m < \sigma_m^{(\chi)}\right)$

$$-\frac{\sigma_a - \sigma_a^{(\chi)}}{\sigma_a^{(\chi)} - \sigma_a^{(\chi_L)}} = \frac{\sigma_m - \sigma_m^{(\chi)}}{\sigma_m^{(\chi_L)} - \sigma_m^{(\chi)}} \tag{4}$$

(IV) compression-dominated zone $\left(\sigma_C \le \sigma_m < \sigma_m^{(\chi_L)}\right)$

$$-\frac{\sigma_a - \sigma_a^{(\chi_L)}}{\sigma_a^{(\chi_L)}} = \left(\frac{\sigma_m - \sigma_m^{(\chi_L)}}{\sigma_C - \sigma_m^{(\chi_L)}}\right)^{2-\psi_{\chi_L}^{k_C}} \tag{5}$$

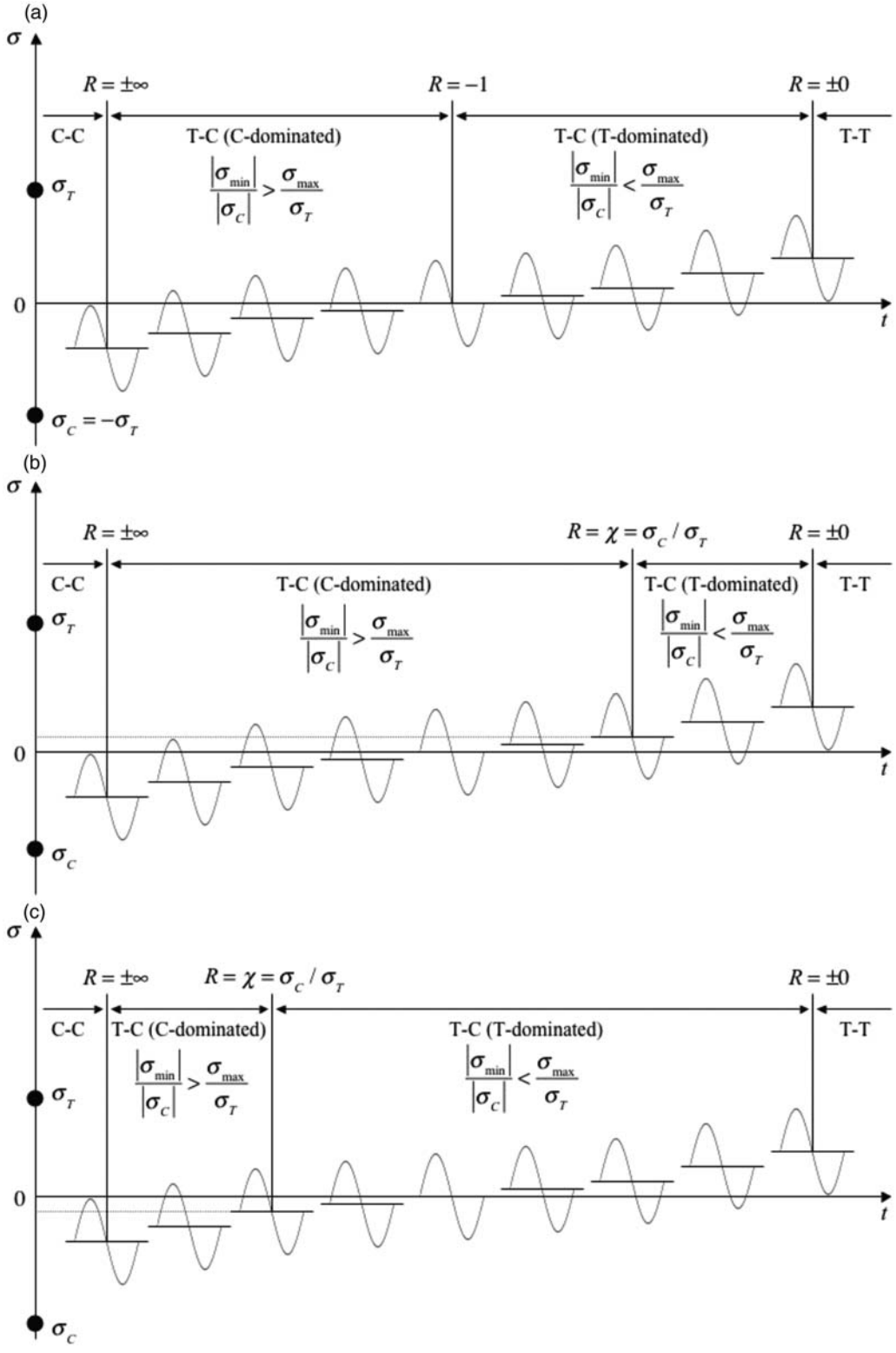

Figure 6. Classification of the mean stress sensitivity in fatigue of composites: (a) classical image for composites with equal strength in tension and compression; (b) non-classical image for composites with larger strength in tension; and (c) non-classical image for composites with larger strength in compression.

where ψ_{χ_R} and ψ_{χ_L} designate the fatigue strength ratios associated with the right and left auxiliary stress ratios, χ_R and χ_L, respectively, and they are defined as

$$\psi_{\chi_R} = \frac{\sigma_{\max}^{(\chi_R)}}{\sigma_T} \tag{6}$$

$$\psi_{\chi_L} = \frac{\sigma_{\min}^{(\chi_L)}}{\sigma_C} \tag{7}$$

The fatigue strength ratios associated with the right and left auxiliary stress ratios are described by means of the monotonic continuous functions of the number of cycles to failure. Note that $\psi_{\chi_R} \in [0, 1]$ and $\psi_{\chi_L} \in [0, 1]$.

The variables $\sigma_a^{(\chi)}$, $\sigma_m^{(\chi)}$, $\sigma_a^{(\chi_R)}$, $\sigma_m^{(\chi_R)}$, $\sigma_a^{(\chi_L)}$, and $\sigma_m^{(\chi_L)}$ represent the alternating stress and mean stress components of the maximum fatigue stresses for fatigue loading at these characteristic stress ratios, and they satisfy the following relations

$$\sigma_a^{(\chi_R)} + \sigma_m^{(\chi_R)} = \sigma_{\max}^{(\chi_R)} \tag{8}$$

$$\sigma_a^{(\chi_L)} + \sigma_m^{(\chi_L)} = \sigma_{\max}^{(\chi_L)} \tag{9}$$

$$\sigma_a^{(\chi)} + \sigma_m^{(\chi)} = \sigma_{\max}^{(\chi)} \tag{10}$$

It should also be reminded that the coordinates $(\sigma_m^{(\chi)}, \sigma_a^{(\chi)})$, $(\sigma_m^{(\chi_R)}, \sigma_a^{(\chi_R)})$, and $(\sigma_m^{(\chi_L)}, \sigma_a^{(\chi_L)})$always fall on the radial straight lines, called the critical and sub-critical lines, with the constant amplitude ratios; i.e.

$$\frac{\sigma_a}{\sigma_m} = \frac{1-\chi}{1+\chi} \tag{11}$$

$$\frac{\sigma_a}{\sigma_m} = \frac{1-\chi_R}{1+\chi_R} \tag{12}$$

$$\frac{\sigma_a}{\sigma_m} = \frac{1-\chi_L}{1+\chi_L} \tag{13}$$

To construct the four-segment anisomorphic CFL diagram for a composite, we need to identify not only the two auxiliary stress ratios but also the reference *S–N* curves associated with the auxiliary stress ratios. In principle, these basic properties should be identified by experiment. According to the non-classical classification of the range of stress ratio that was discussed above, it is a good practice to assume that $\chi_R = 0$ and $\chi_L = -\infty$ since these values of auxiliary stress ratios correspond to the borders between T–T and T–C loading and between C–C and T–C loading, respectively. The implementation according to this assumption is hereafter called the *standard* four-segment anisomorphic CFL diagram. A question is raised concerning the fatigue data for the standard auxiliary stress ratios that are required to identify the associated reference *S–N* curves. While they can be obtained by experiment, those fatigue data are not always available in the established database in general. However, this problem can easily be bypassed; namely, the fatigue strengths for constant values of life that are associated with the standard auxiliary stress ratios can approximately be identified by extrapolating the linear CFL envelopes plotted on the T–T segment $[\sigma_m^{(R=0.1)}, \sigma_T]$ and on the C–C segment $[\sigma_C, \sigma_m^{(R=10)}]$, respectively. The requirement of these additional data for constructing the four-segment anisomorphic CFL diagram reduces the simplicity of the two-segment anisomorphic CFL diagram. Instead, the four-segment anisomorphic CFL diagram approach gains amplified flexibility that allows accurately describing a highly non-linear and asymmetric CFL diagram for the matrix-dominated fatigue failure of composites.

Note that if either of the two auxiliary stress ratios is assumed to coincide with the critical stress ratio, the four-segment model is reduced to the three-segment model that has been tested in an earlier study.[43] Obviously, it also reduces to the original two-segment model[24,25] if both of the two auxiliary stress ratios agree with the critical stress ratio and thus the associated transitional segments both disappear. It may incidentally be remarked that when referring to the standard three-segment anisomorphic CFL diagram, we implicitly assume that the second critical stress ratio is given by either of the standard auxiliary stress ratios; i.e. $\chi_S = \chi_R = 0$ or $\chi_S = \chi_L = -\infty$. The examples of the standard three-segment anisomorphic CFL diagram have actually been presented in Figure 4.

The exponents k_T and k_C were introduced so that the four-segment anisomorphic CFL diagram can be reduced to the modified two-segment anisomorphic CFL diagram[49] that is furnished with a capability to adjust the rate of change in the shape of CFL curve from a straight line to a parabola on the tension-dominated and compression-dominated segments, respectively. When applying the standard four-segment anisomorphic CFL diagram, however, we may approximately assume that $k_T = k_C = 1$.

It should incidentally be remarked that for a particular loading condition or a particular composite, we could use one of the reduced versions of the anisomorphic CFL diagram appropriately instead of the most general four-segment version. If we assume the four-segment anisomorphic CFL diagram for any case, however, we are free of selection of a version and always able to feel secure about the accuracy of description of highly distorted CFL diagrams.

Procedure for constructing the four-segment anisomorphic CFL diagram

The construction procedure is explained in more detail. To construct the four-segment anisomorphic CFL diagram, we need to evaluate the coordinates $(\sigma_m^{(\chi)}, \sigma_a^{(\chi)})$, $(\sigma_m^{(\chi_R)}, \sigma_a^{(\chi_R)})$, and $(\sigma_m^{(\chi_L)}, \sigma_a^{(\chi_L)})$ for a given constant value of life N_f. Once they are known, we can draw the associated CFL envelope using the piecewise-defined functions given by equations (2) to (5). To draw a CFL envelope for a given constant value of life, we take the following steps:

1. Evaluate the tensile strength $\sigma_T > 0$ and compressive strength $\sigma_C < 0$ of the composite.
2. Calculate the value of the critical stress ratio $\chi = \sigma_C/\sigma_T$ (< 0).
3. Perform constant amplitude tension–compression fatigue tests at the critical stress ratio $R = \chi$ to obtain the reference S–N data.
4. Identify the normalized reference S–N curve for the critical stress ratio using the fatigue strength ratio

$$\psi_\chi = \frac{\sigma_{\max}^{(\chi)}}{\sigma_T} \tag{14}$$

Then, fit an analytical function

$$2N_f^{(\chi)} = f(\psi_\chi) \tag{15}$$

to the normalized reference S–N curve for the critical stress ratio. For fitting in this study, we assume the following function

$$f(x) = \frac{1}{K^*}\frac{1}{x^n}\frac{\langle 1-x\rangle^a}{\left\langle x - x_{(L)}\right\rangle^b} \tag{16}$$

where the angular brackets $\langle\rangle$ denote the singular function defined as $\langle x\rangle = \max\{0, x\}$. The material constants K^*, n, a, b, and $\psi_{\chi(L)}$ are determined by fitting equation (15) to the reference fatigue data for the critical stress ratio.

5. Perform constant amplitude fatigue tests at the right and left auxiliary stress ratios $\chi_R = 0$ and $\chi_L = -\infty$, respectively, to obtain additional reference S–N data.
6. Identify the normalized reference S–N curves for the auxiliary stress ratios by fitting the following functions to the additional reference S–N data following the same procedure as in 4.

$$2N_f^{(\chi_R)} = f(\psi_{\chi_R}) \tag{17}$$
$$2N_f^{(\chi_L)} = f(\psi_{\chi_L}) \tag{18}$$

6. Calculate the coordinates $(\sigma_m^{(\chi)}, \sigma_a^{(\chi)})$, $(\sigma_m^{(\chi_R)}, \sigma_a^{(\chi_R)})$, and $(\sigma_m^{(\chi_L)}, \sigma_a^{(\chi_L)})$ for a given constant value of life N_f.

$$\begin{Bmatrix} \sigma_m^{(\chi)}(N_f) \\ \sigma_a^{(\chi)}(N_f) \end{Bmatrix} = \frac{1}{2}\psi_\chi(N_f)\sigma_T \begin{Bmatrix} 1+\chi \\ 1-\chi \end{Bmatrix} \tag{19}$$

$$\begin{Bmatrix} \sigma_m^{(\chi_R)}(N_f) \\ \sigma_a^{(\chi_R)}(N_f) \end{Bmatrix} = \frac{1}{2}\psi_{\chi_R}(N_f)\sigma_T \begin{Bmatrix} 1+\chi_R \\ 1-\chi_R \end{Bmatrix} \tag{20}$$

$$\begin{Bmatrix} \sigma_m^{(\chi_L)}(N_f) \\ \sigma_a^{(\chi_L)}(N_f) \end{Bmatrix} = \frac{1}{2}\psi_{\chi_L}(N_f) \begin{Bmatrix} \left(1+\frac{1}{\chi_L}\right)\sigma_C \\ \left(1-\frac{1}{\chi_L}\right)|\sigma_C| \end{Bmatrix} \tag{21}$$

7. Draw the CFL envelope associated with the constant value of life N_f using the piecewise-defined CFL functions given by equations (2) to (5).
8. Repeat the steps from 6 to 7 for different constant values of fatigue life.
9. End the construction procedure with wrapping the CFL envelopes in the profile defined by

$$\sigma_a + \sigma_m = \sigma_T \tag{22}$$
$$\sigma_a - \sigma_m = \sigma_C \tag{23}$$

If the fatigue data for the stress ratios that are close to the standard auxiliary stress ratios, for example $R = 0.1$ and $R = 10$, are available, we can use them for construction of the four-segment anisomorphic CFL diagram; namely, the normalized S–N curves for $R = 0.1$ and $R = 10$ are identified, respectively, by fitting the following functions to those S–N data available after normalization.

$$2N_f^{(0.1)} = f(\psi_{0.1}) = f\left(\frac{\sigma_{\max}^{(0.1)}}{\sigma_T}\right) \tag{24}$$

$$2N_f^{(10)} = f(\psi_{10}) = f\left(\frac{\sigma_{\min}^{(10)}}{\sigma_C}\right) \tag{25}$$

Using these normalized S–N curves for $R = 0.1$ and $R = 10$, the coordinates $(\sigma_m^{(0.1)}, \sigma_a^{(0.1)})$ and $(\sigma_m^{(10)}, \sigma_a^{(10)})$ are calculated for the given constant value of life N_f. Then, the coordinates $(\sigma_m^{(\chi_R=0)}, \sigma_a^{(\chi_R=0)})$ and $(\sigma_m^{(\chi_L=\infty)}, \sigma_a^{(\chi_L=\infty)})$ for the given constant value of life N_f are evaluated by extrapolating the linear envelopes assumed on the intervals $[\sigma_m^{(0.1)}, \sigma_T]$ and $[\sigma_C, \sigma_m^{(10)}]$, respectively. The remaining steps are the same as described above.

Application of the standard four-segment anisomorphic CFL model

The off-axis CFL diagrams described using the standard four-segment CFL diagram approach are shown in

Figures 7 to 12 for all the fiber orientations, respectively. The off-axis *S–N* relationships predicted using the off-axis CFL diagrams are presented in Figures 13 to 18, respectively. Following the procedure mentioned above, the reference fatigue strengths associated with the standard auxiliary stress ratios $\chi_R = 0$ and $\chi_L = -\infty$ were evaluated by linear extrapolation of the linear CFL envelopes on the T–T and C–C loading segments $\left[\sigma_m^{(R=0.1)}, \sigma_T\right]$ and $\left[\sigma_C, \sigma_m^{(R=10)}\right]$, respectively. The material constants that characterize the normalized reference *S–N* curves for the critical and auxiliary stress ratios are presented in Table 4.

From Figures 7 to 12, it is seen that the full shapes of off-axis CFL diagrams for the unidirectional CFRP laminate can accurately be described by means of the standard four-segment anisomorphic CFL diagram approach, regardless of fiber orientation. As expected, the right and left transitional segments accommodate the generalized anisomorphic CFL diagram to a large change in mean stress sensitivity from a high level in tension-dominated fatigue loading to a low level in compression-dominated fatigue loading, and thus, the addition of these transitional segments to the anisomorphic CFL diagram greatly improves the predictive accuracy.

In Figures 13 to 18, the solid curves indicate the predicted *S–N* relationships and the dashed curves the reference *S–N* curves that were identified by fitting equations (15), (24), and (25) to the associated fatigue data. From these figures, it can be observed that overall good predictions of the off-axis *S–N* relationships have been obtained. Due to the linear interpolation of CFL envelopes on each of the four segments, slightly conservative predictions of the off-axis *S–N* relationships for the unidirectional CFRP laminate were obtained, regardless of stress ratio and fiber orientation, except for the slightly optimistic prediction only for $\theta = 45^\circ$ at $R = 0.5$.

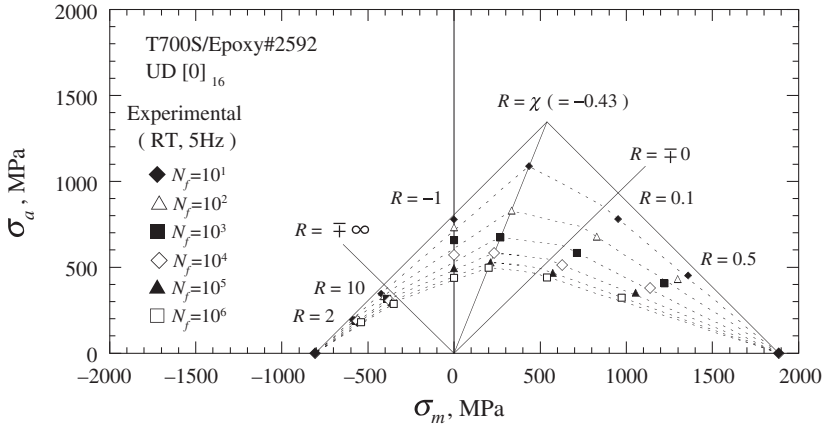

Figure 7. Off-axis CFL diagrams predicted using the four-segment anisomorphic CFL diagram approach ($\theta = 0^\circ$).

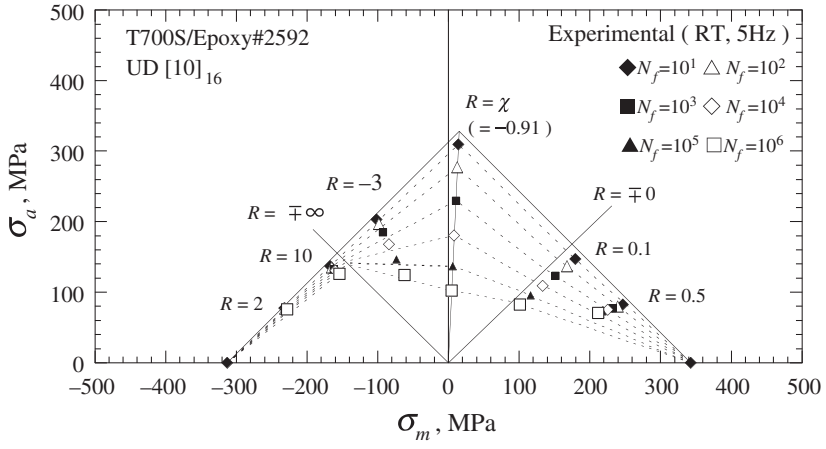

Figure 8. Off-axis CFL diagrams predicted using the four-segment anisomorphic CFL diagram approach ($\theta = 10^\circ$).

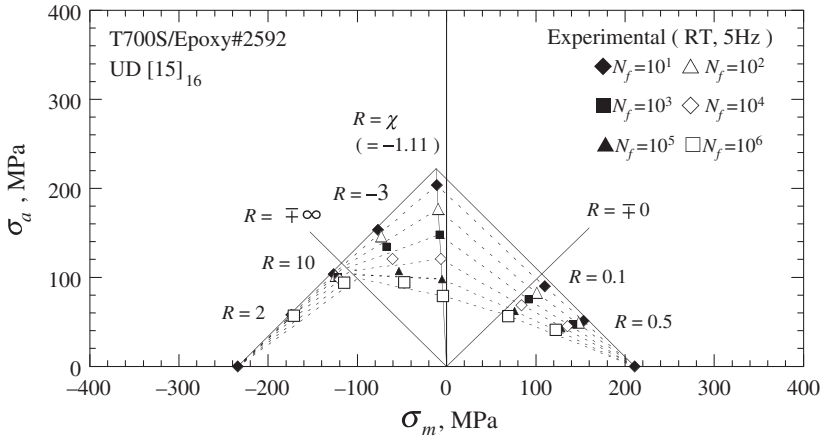

Figure 9. Off-axis CFL diagrams predicted using the four-segment anisomorphic CFL diagram approach ($\theta = 15°$).

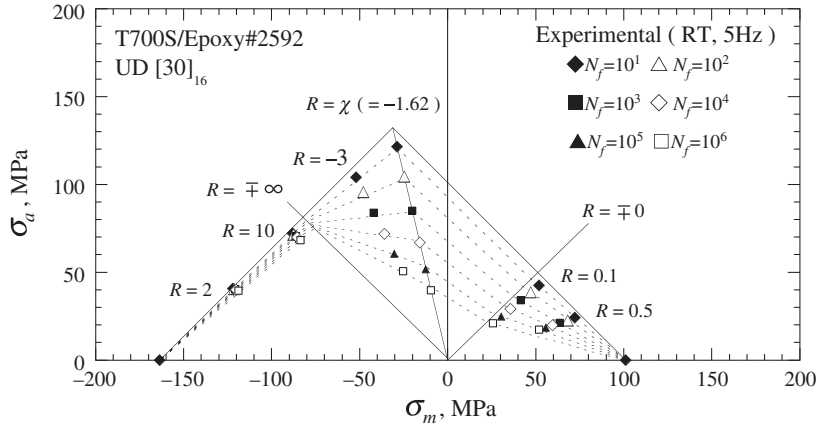

Figure 10. Off-axis CFL diagrams predicted using the four-segment anisomorphic CFL diagram approach ($\theta = 30°$).

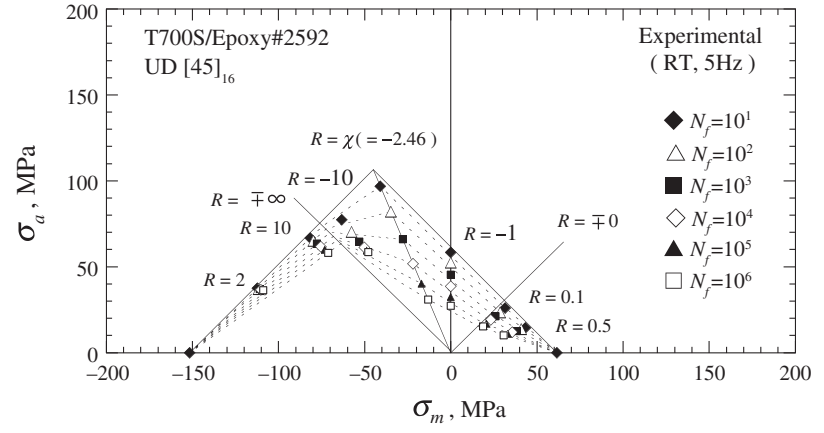

Figure 11. Off-axis CFL diagrams predicted using the four-segment anisomorphic CFL diagram approach ($\theta = 45°$).

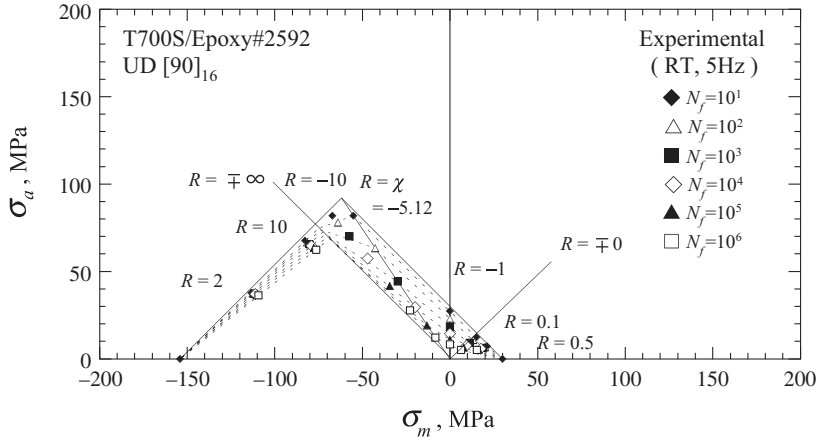

Figure 12. Off-axis CFL diagrams predicted using the four-segment anisomorphic CFL diagram approach ($\theta = 90^\circ$).

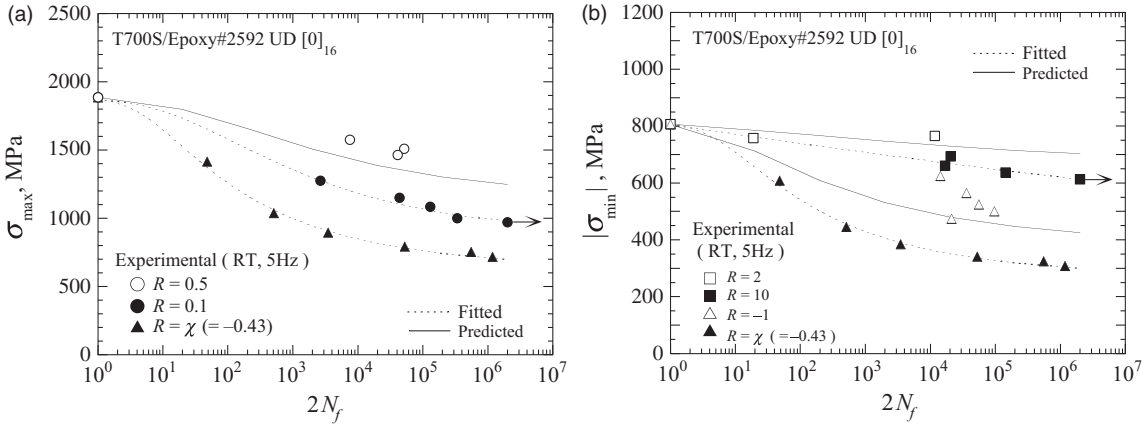

Figure 13. Off-axis *S–N* relationships predicted using the three-segment anisomorphic CFL diagram approach ($\theta = 0^\circ$): (a) $R = \chi$, 0.1, and 0.5 and (b) $R = 2$, 10, -1, and χ.

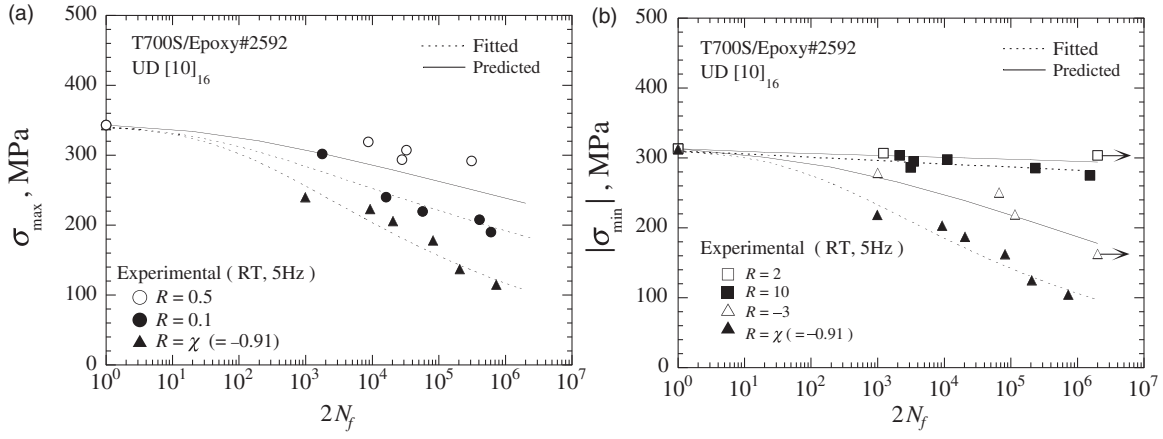

Figure 14. Off-axis *S–N* relationships predicted using the three-segment anisomorphic CFL diagram approach ($\theta = 10^\circ$): (a) $R = \chi$, 0.1, and 0.5 and (b) $R = 2$, 10, -3, and χ.

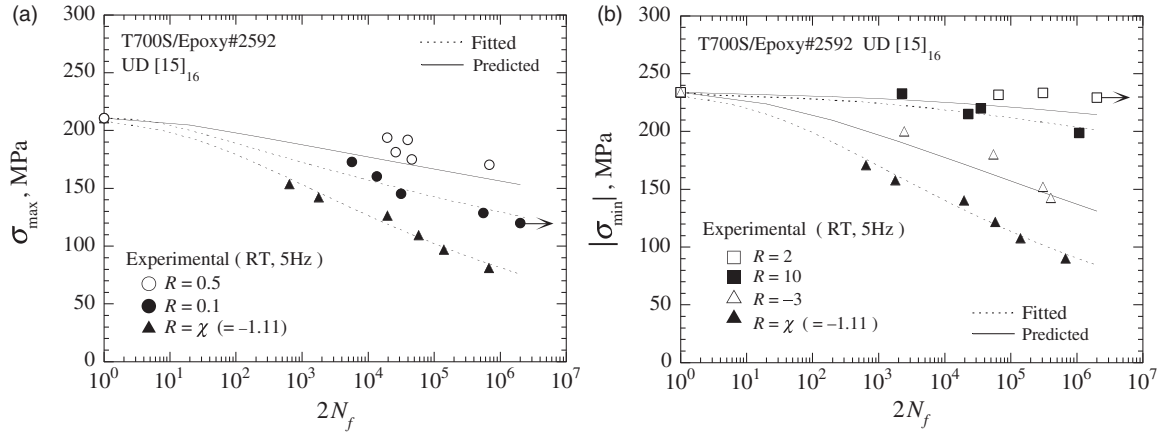

Figure 15. Off-axis *S–N* relationships predicted using the three-segment anisomorphic CFL diagram ($\theta = 15°$): (a) $R = \chi$, 0.1, and 0.5 and (b) $R = 2$, 10, -3, and χ.

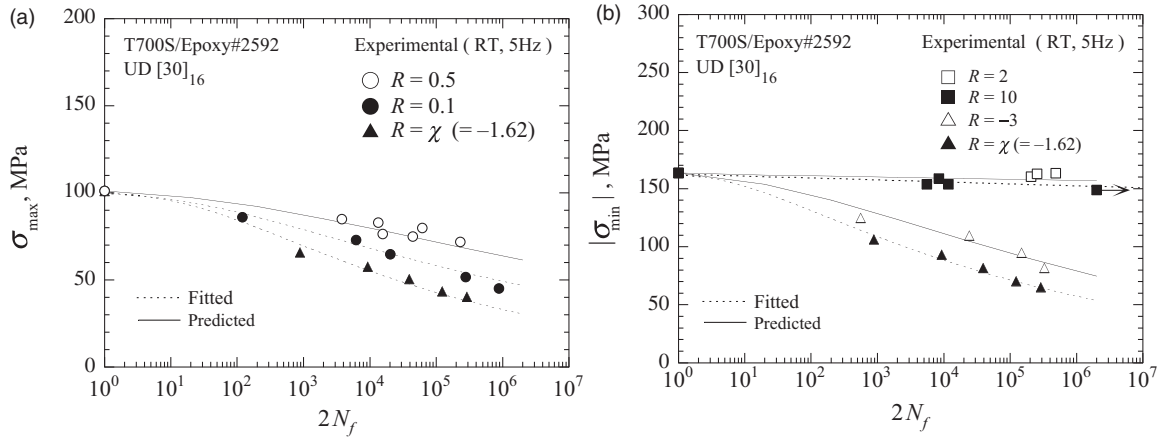

Figure 16. Off-axis *S–N* relationships predicted using the three-segment anisomorphic CFL diagram ($\theta = 30°$): (a) $R = \chi$, 0.1, and 0.5 and (b) $R = 2$, 10, -3, and χ.

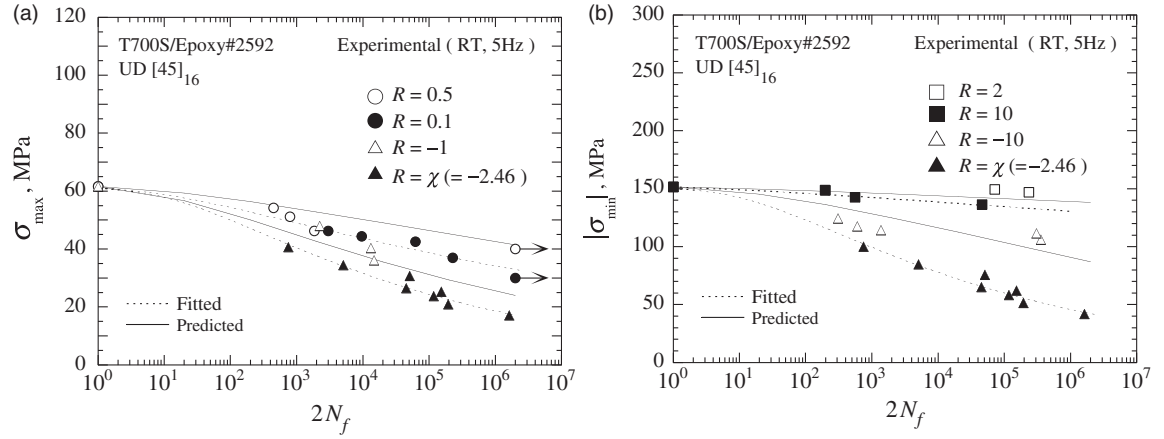

Figure 17. Off-axis *S–N* relationships predicted using the three-segment anisomorphic CFL diagram ($\theta = 45°$): (a) $R = \chi$, -1, 0.1, and 0.5 and (b) $R = 2$, 10, -10, and χ.

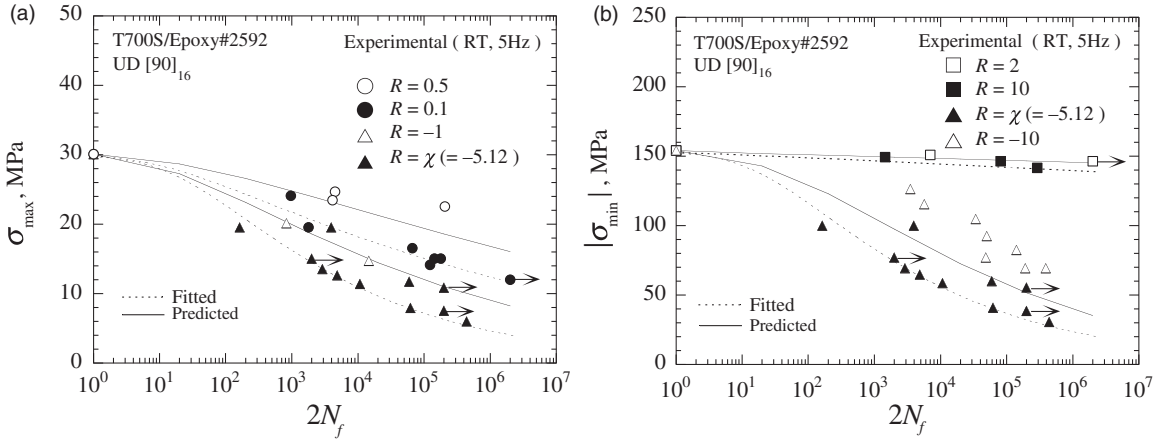

Figure 18. Off-axis *S–N* relationships predicted using the three-segment anisomorphic CFL diagram approach ($\theta = 90°$): (a) $R = \chi$, -1, 0.1, and 0.5 and (b) $R = 2$, 10, -10, and χ.

Table 4. Material constants that characterize the normalized reference *S–N* curves for the critical and auxiliary stress ratios.

Off-axis angle (°)	Stress ratio, *R*	*K**/2	*n*	*a*	*b*	x_L
0	0.1	0.19	2	1	3.6	0.48
	$\chi = -0.43$	0.98	−3	0.6	5.3	0.33
	10	2	53	0	0	0
10	0.1	0.002	14	1.5	0	0
	$\chi = -0.91$	0.002	7	1.5	0	0
	10	2	140	0.3	0	0
15	0.1	0.1	8	0.4	15	0
	$\chi = -1.11$	0.02	10	1	0	0
	10	0.0000001	30	3.5	0	0
30	0.1	0.005	10	1.5	1.5	0.15
	$\chi = -1.62$	0.05	10	0.8	0	0
	10	0.1	190	1	0	0
45	0.1	0.02	17	1	0	0
	$\chi = -2.46$	0.02	8	1	0	0
	10	0.01	70	1	0	0
90	0.1	0.02	11	1	0	0
	$\chi = -5.12$	0.02	5	1	0	0
	10	0.01	120	1.4	0	0

Finally, it is emphasized that the proposed four-segment anisomorphic CFL diagram can distinguish between tensile and compressive failure under different modes of loading, and thus, it can indirectly take into account the different mechanisms of fatigue failure. As observed in this study, the proposed four-segment anisomorphic CFL diagram can accurately describe the highly non-linear and asymmetric CFL diagrams for the unidirectional carbon/epoxy laminate in any off-axis fiber orientations. Accordingly, it can be used to accurately describe the CFL diagrams for fatigue loading in the principal directions of the unidirectional composite. As suggested earlier in 'Introduction', the principal anisomorphic CFL diagrams for a given unidirectional composite can be used to non-analytically evaluate the reduction in strength in the principal strengths with fatigue loading at any stress ratio. The use of the generalized four-segment anisomorphic CFL diagram for that purpose allows us to develop a new multiaixal fatigue life prediction methodology for composites that is based on a multiaxial fatigue failure criterion and the principal anisomorphic CFL diagrams.

Conclusions

The effect of fiber orientation on the full shape of the off-axis CFL diagram for a unidirectional carbon/epoxy laminate was examined. The two-segment and three-segment anisomorphic CFL diagram approaches were tested for the accuracy of prediction of the off-axis CFL diagrams observed by experiment. A most general four-segment version of the anisomorphic CFL diagram approach that allows accurate prediction of highly non-linear and asymmetric CFL diagram for a composite was developed. The validity of the proposed four-segment anisomorphic CFL diagram approach was evaluated by comparing the predicted and experimental CFL diagrams for the unidirectional composite in different fiber orientations. The results obtained can be summarized as follows:

1. The off-axis CFL diagram for the unidirectional CFRP laminate becomes asymmetric about the

alternating stress axis, regardless of fiber orientation. The asymmetry in off-axis CFL diagram depends on fiber orientation, and it correlates with the asymmetry in static strength in tension and compression.
2. It is suggested that the profile of the off-axis CFL diagram in a given fiber orientation has its peak at a positive mean stress in the first quadrant of the alternating stress versus mean stress plane if the off-axis tensile strength is larger than the off-axis compressive strength (e.g. $\theta = 0^\circ$ and 10°); otherwise, it appears at a negative mean stress in the second quadrant (e.g. $\theta = 15^\circ$, 30°, 45° and 90°).
3. There is a strong tendency that the on-axis CFL envelopes for the fiber direction have peaks under fatigue loading at the critical stress ratio that is equal to the ratio of off-axis compressive strength to off-axis tensile strength over the range of fatigue life tested in this study. The CFL envelopes in a direction inclined at an angle to the transverse direction have the same feature up to a certain value of life, but in the range beyond it, they are apt to have peaks nearly at $R = -\infty$. Such a transition in peak position of a CFL envelope occurs earlier in life as the off-axis angle increases, and thus, the CFL envelope is apt to incline more significantly to the left of the alternating stress axis.
4. The gradient of off-axis S–N relationship becomes larger under fatigue loading at the critical stress ratio, regardless of fiber orientation. This feature suggests that the unidirectional CFRP laminate exhibits highest sensitivity to off-axis fatigue, and thus degrades more significantly, under cyclic loading at the critical stress ratio, regardless of fiber orientation. There is a strong correlation between the rapid degradation and the larger alternating stress during fatigue loading at the critical stress ratio.
5. The two-segment anisomorphic CFL diagram approach is applicable to the unidirectional CFRP laminate subjected to fatigue loading in the fiber direction ($\theta = 0^\circ$). However, it fails to accurately predict the CFL diagrams for the matrix-dominated off-axis and transverse fatigue behaviors, because of a significant difference between the mean stress sensitivities in fatigue under tension-dominated and compression-dominated fatigue loading conditions. The latter suggests that the use of fatigue data only for the critical stress ratio is insufficient to accurately describe the CFL diagrams for the matrix-dominated fatigue behavior of composites.
6. The three-segment anisomorphic CFL model that assumes a transitional segment to the left of the critical line succeeds in accommodating itself to a significant change in mean stress sensitivity in off-axis fatigue, and thus greatly improves the accuracy of description of the off-axis CFL diagram for the unidirectional CFRP laminate, regardless of fiber orientation.
7. A generalized four-segment anisomorphic CFL diagram for unidirectional composites was developed on the basis of the non-classical classification of the range of mean stress sensitivity in fatigue of composites that assumes distinguishing between different modes of failure and loading. The failure-mode based four-segment anisomorphic CFL diagram developed in this study has the potential of accurately describing the highly non-linear and asymmetric off-axis CFL diagram for the unidirectional CFRP laminate over the whole range of mean stress, regardless of fiber orientation. It is worth testing in more quantitative terms on the basis of more experimental data.

Funding

This study was supported in part by the Ministry of Education, Culture, Sports, Science and Technology of Japan under a Grant-in-Aid for Scientific Research (no. 20360050).

Conflict of interest

None declared.

References

1. Boller KH. Fatigue properties of fibrous glass-reinforced plastics laminates subjected to various conditions. *Mod Plast* 1957; 34: 163–186 (293).
2. Boller KH. Fatigue characteristics of RP laminates subjected to axial loading. *Mod Plast* 1964; 41: 145–150 (188).
3. Owen MJ and Bishop PT. Fatigue properties of glass-reinforced plastics containing a stress concentrator. *J Phys D: Applied Physics* 1973; 6: 2057–2069.
4. Curtis PT. The fatigue behaviour of fibrous composite materials. *J Strain Anal* 1989; 24(4): 235–244.
5. Curtis DC, Moore DR, Slater B, et al. Fatigue testing of multi-angle laminates of CF/PEEK. *Composites* 1988; 19(6): 446–452.
6. Salkind MJ. Fatigue of composites. In: Corten HT (ed) *Composite materials: testing and design (second conference)*, Anaheim, CA, 20–22 April 1971, ASTM STP 497, pp.143–169. Philadelphia, PA: ASTM, 1972.
7. Hahn HT. Fatigue behavior and life prediction of composite laminates. In: Tsai SW (ed) *Composite materials: testing and design (fifth conference)* New Orleans, LA, 20–22 March 1978, ASTM STP 674, pp.383–417. Philadelphia, PA: ASTM, 1979.
8. El-Kadi H and Ellyin F. Effect of stress ratio on the fatigue of unidirectional glass fibre/epoxy composite laminae. *Composites* 1994; 25: 917–924.
9. Kawai M and Suda H. Effects of non-negative mean stress on the off-axis fatigue behavior of unidirectional carbon/epoxy composites at room temperature. *J Compos Mater* 2004; 38(10): 833–854.

10. Kawai M. A phenomenological model for off-axis fatigue behavior of unidirectional polymer matrix composites under different stress ratios. *Composites Part A* 2004; 35(7–8): 955–963.
11. Harris B (ed.) *Fatigue in composites*. Cambridge: Woodhead Publishing Limited, 2003.
12. Kawai M. Fatigue life prediction of composite materials under constant amplitude loading. In: Vassilopoulos AP (ed.) *Fatigue life prediction of composites and composite structures*. UK: Woodhead Publishing Limited, 2010, pp.177–219.
13. Ansell MP, Bond IP and Bonfield PW. Constant life diagrams for wood composites and polymer matrix composites. In: *Proceedings of 9th international conference on composite materials (ICCM 9)*, Madrid, Spain, 12–16 July 1993, Vol. V, pp.692–699.
14. Harris B, Reiter H, Adam T, et al. Fatigue behaviour of carbon fibre reinforced plastics. *Composites* 1990; 21(3): 232–242.
15. Adam T, Gathercole N, Reiter H, et al. Fatigue life prediction for carbon fibre composites. *Adv Compos Lett* 1992; 1: 23–26.
16. Gathercole N, Reiter H, Adam T, et al. Life prediction for fatigue of T800/5245 carbon-fibre composites: I. constant-amplitude loading. *Fatigue* 1994; 16: 523–532.
17. Harris B, Gathercole N, Lee JA, et al. Life-prediction for constant-stress fatigue in carbon-fibre composites. *Philos Trans R Soc London* 1997; A355: 1259–1294.
18. Beheshty MH, Harris B and Adam T. An empirical fatigue-life model for high-performance fibre composites with and without impact damage. *Composites Part A* 1999; 30: 971–987.
19. Ramani SV and Williams DP. Notched and unnotched fatigue behavior of angle-ply graphite/epoxy composites. In: Reifsnider KL and Lauraitis KN (eds) *Fatigue of filamentary composite materials*, Denver, CO, 15–16 November 1976, ASTM STP 636, pp.27–46. Lutherville-Timonium, MD: ASTM, 1977.
20. Goodman J. *Mechanics applied to engineering*. UK: Longman Green, 1899.
21. Mandell JF, Samborsky DD, Wang L, et al. New fatigue data for wind turbine blade materials. *Trans ASME, J Sol Energy Eng* 2003; 125: 506–514.
22. Sutherland HJ and Mandell JF. Optimized constant-life diagram for the analysis of fiberglass composites used in wind turbine blade. *Trans ASME, J Sol Energy Eng* 2005; 127: 563–569.
23. Adam T, Fernando G, Dickson RF, et al. Fatigue life prediction for hybrid composites. *Int J Fatigue* 1989; 11(4): 233–237.
24. Kawai M. A method for identifying asymmetric dissimilar constant fatigue life diagrams of CFRP laminates. In: *Proceedings of the fifth Asian–Australasian conference on composite materials (ACCM-5)*, Hong Kong, 27–30 November, 2006; *Key Eng Mater* 2007; 334–335:61–64.
25. Kawai M and Koizumi M. Nonlinear constant fatigue life diagram for carbon/epoxy laminates at room temperature. *Composites Part A* 2007; 38: 2342–2353.
26. Vassilopoulos AP, Manshadi BD and Keller T. Piecewise non-linear constant life diagram formulation for FRP composite materials. *Int J Fatigue* 2010; 32: 1731–1738.
27. Kawai M and Maki N. Fatigue strength of cross-ply CFRP laminates at room and high temperatures and its phenomenological modeling. *Int J Fatigue* 2006; 28(10): 1297–1306.
28. Kawai M and Honda N. Off-axis fatigue behavior of a carbon/epoxy cross-ply laminate and predictions considering inelasticity and in-situ strength of embedded plies. *Int J Fatigue* 2008; 30(10–11): 1743–1755.
29. Hashin Z and Rotem A. A fatigue failure criterion for fiber-reinforced materials. *J Compos Mater* 1973; 7: 448–464.
30. Sims DF and Brogdon VH. Fatigue behavior of composites under different loading modes. In: Reifsnider KL and Lauraitis KN (eds) *Fatigue of filamentary composite materials*, Denver, CO, 15–16 November 1976, ASTM STP 636, pp.185–205. Lutherville-Timonium, MD: ASTM, 1977.
31. Ellyin F and El-Kadi H. A fatigue failure criterion for fiber reinforced composite laminate. *Compos Struct* 1990; 15: 61–74.
32. Awerbuch J and Hahn HT. Off-axis fatigue of graphite/epoxy composite. ASTM STP 723, 1981, pp.243–273.
33. Fawaz Z and Ellyin F. Fatigue failure model for fibre-reinforced materials under general loading conditions. *J Compos Mater* 1994; 28(15): 1432–1451.
34. Kawai M, Yajima S, Hachinohe A, et al. Off-axis fatigue behavior of unidirectional carbon fiber-reinforced composites at room and high temperatures. *J Compos Mater* 2001; 35(7): 545–576.
35. Kawai M, Yajima S, Hachinohe A, et al. High-temperature off-axis fatigue behaviour of unidirectional carbon fiber-reinforced composites with different resin matrices. *Compos Sci Technol* 2001; 61: 1285–1302.
36. Philippidis TP and Vassilopoulos AP. Complex stress state effect on fatigue life of GRP laminates, Part I, experimental. *Int J Fatigue* 2002; 24: 813–823.
37. Philippidis TP and Vassilopoulos AP. Complex stress state effect on fatigue life of GRP laminates. Part II, theoretical formulation. *Int J Fatigue* 2002; 24: 825–830.
38. JIS K7073. Testing method for tensile properties of carbon fiber-reinforced plastics, Japanese Industrial Standard, Japanese Standards Association, 1988.
39. JIS K7083. Testing method for constant-load amplitude tension-tension fatigue of carbon fibre reinforced plastics, Japanese Industrial Standard, Japanese Industrial Association, 1993.
40. JIS K7076. Testing method for compressive properties of carbon fiber-reinforced plastics, Japanese Industrial Standard, Japanese Industrial Association, 1991.
41. Haberle JG and Matthews FL. An improved technique for compression testing of unidirectional fibre-reinforced plastics; development and results. *Composites Part A* 1994; 25(5): 358–371.
42. Kawai M and Saito S. Off-axis strength differential effects in unidirectional carbon/epoxy laminates at different strain rates and predictions of associated failure envelopes. *Composites Part A* 2009; 40: 1632–1649.

43. Kawai M and Murata T. A three-segment anisomorphic constant life diagram for the fatigue of symmetric angle-ply carbon/epoxy laminates at room temperature. *Composites Part A* 2010; 41: 1498–1510.
44. Mall S, Katwyk DW, Bolick RL, et al. Tension-compression fatigue behavior of a H-VARTM manufactured unnotched and notched carbon/epoxy composite. *Compos Struct* 2009; 90: 201–207.
45. Rotem A and Nelson HG. Failure of a laminated composite under tension-compression fatigue loading. *Compos Sci Technol* 1989; 36: 45–62.
46. Rosenfeld MS and Huang SL. Fatigue characteristics of graphite/epoxy laminates under compression loading. *J Aircr* 1978; 15(5): 264–268.
47. Gamstedt EK and Sjogren BA. Micromechanisms in tension-compression fatigue of composite laminates containing transverse plies. *Compos Sci Technol* 1999; 59: 167–178.
48. Rotem A. The fatigue behavior of composite laminates under various mean stresses. *Compos Struct* 1991; 17: 113–126.
49. Kawai M, Shiratsuchi T and Yang K. A spectrum fatigue life prediction method based on the nonlinear constant fatigue life diagram for CFRP laminates. In: *Proceedings of 6th Asia-Australasian conference on composite materials (ACCM-6)*, Kumamoto, Japan, 23–26 September 2008, pp.153–156.